IOPscience iopscience.iop.org

Home Search Collections Journals About Contact us My IOPscience

A light-trapping strategy for nanocrystalline silicon thin-film solar cells using three-dimensionally assembled nanoparticle structures

This content has been downloaded from IOPscience. Please scroll down to see the full text.

2016 Nanotechnology 27 055403

(http://iopscience.iop.org/0957-4484/27/5/055403)

View the table of contents for this issue, or go to the journal homepage for more

Download details:

IP Address: 143.248.144.56
This content was downloaded on 16/06/2016 at 15:30

Please note that terms and conditions apply.

IOP Publishing Nanotechnology
Nanotechnology 27 (2016) 055403 (8pp) doi:10.1088/0957-4484/27/5/055403

A light-trapping strategy for nanocrystalline silicon thin-film solar cells using three-dimensionally assembled nanoparticle structures

Kyungyeon Ha[1,2], Eunseok Jang[3], Segeun Jang[1,2], Jong-Kwon Lee[2], Min Seok Jang[2], Hoseop Choi[1,2], Jun-Sik Cho[3] and Mansoo Choi[1,2]

[1] School of Mechanical and Aerospace Engineering, Seoul National University, Seoul 08826, Korea
[2] Global Frontier Center for Multiscale Energy System, Seoul National University, Seoul 08826, Korea
[3] Photovoltaic Laboratory, Korea Institute of Energy Research, Daejeon 34129, Korea

E-mail: mchoi@snu.ac.kr and jscho@kier.re.kr

Received 2 October 2015, revised 27 November 2015
Accepted for publication 1 December 2015
Published 11 January 2016

Abstract

We report three-dimensionally assembled nanoparticle structures inducing multiple plasmon resonances for broadband light harvesting in nanocrystalline silicon (nc-Si:H) thin-film solar cells. A three-dimensional multiscale (3DM) assembly of nanoparticles generated using a multi-pin spark discharge method has been accomplished over a large area under atmospheric conditions via ion-assisted aerosol lithography. The multiscale features of the sophisticated 3DM structures exhibit surface plasmon resonances at multiple frequencies, which increase light scattering and absorption efficiency over a wide spectral range from 350–1100 nm. The multiple plasmon resonances, together with the antireflection functionality arising from the conformally deposited top surface of the 3D solar cell, lead to a 22% and an 11% improvement in power conversion efficiency of the nc-Si:H thin-film solar cells compared to flat cells and cells employing nanoparticle clusters, respectively. Finite-difference time-domain simulations were also carried out to confirm that the improved device performance mainly originates from the multiple plasmon resonances generated from three-dimensionally assembled nanoparticle structures.

S Online supplementary data available from stacks.iop.org/NANO/27/055403/mmedia

Keywords: multiple plasmon resonances, three-dimensional nanostructure, light trapping, thin-film solar cells, nanoparticle assembly

(Some figures may appear in colour only in the online journal)

1. Introduction

Thin-film solar cells provide the benefits of reduced material and fabrication costs, higher flexibility and lower weight in comparison to crystalline silicon (Si) solar cells [1]. Hydrogenated nanocrystalline Si (nc-Si:H) is of considerable interest in thin-film solar cells because of its superior long-wavelength response (a band gap of 1.1 eV) and stability against light soaking. However, there still remain the challenges of enhancing light absorption in the red and near-infrared regions (due to the nature of the indirect transition in nc-Si:H) and improving the productivity of solar cells (due to the low deposition rate of nc-Si:H). To realize high-efficiency and low-cost solar cells, a light-trapping strategy is crucial because it allows the enhancement of light absorption [2–4] and the reduction of the thickness of the nc-Si:H [5], simultaneously. Various plasmonic light-trapping techniques for thin-film solar cells have been developed; however, most of

 © 2016 IOP Publishing Ltd Printed in the UK

these studies have focused on rather simple-shaped nanostructures [6], including nanoparticles [7, 8], nanowires [9, 10], and nanobumps [11–14], which usually possess surface plasmon resonances at a specific frequency, and thus exhibit the light-trapping effect in a rather narrow spectral range. Researchers have recently reported a way to obtain light trapping in a broader spectrum using two different types of plasmonic nanostructures. For instance, a single or two metallic nanoparticles have been incorporated into a single [15, 16] or dual [17, 18] interfacial layer of thin-film solar cells. A hybrid approach of surface plasmonic resonances (from nanogratings) and localized plasmonic resonances (from nanoparticles) has been also introduced [19]. Three-dimensional multiscale (3DM) structures can further extend the spectral range of light trapping by generating plasmon resonances at multiple frequencies originating from their multiscale geometry. However, 3D plasmonic structures have rarely been investigated due to difficulties in fabrication. Ion-assisted aerosol lithography (IAAL) [20–29] of metal nanoparticles generated using a multi-pin spark discharge method [27, 30] enables the uniform and reproducible 3DM assembly of nanoparticles with nanoscale-resolution controllability over the wafer scale at room temperature and atmospheric pressure. This cost-effective 3DM fabrication method also ensures compatibility with other building block materials and various solar cell fabrication processes.

In this study, we fabricated 3DM structure arrays using IAAL with a multi-pin spark discharge method under atmospheric conditions to induce multiple plasmon resonances for trapping a broad spectrum of light. We successfully demonstrated multiple plasmon resonances in the fabricated 3DM structures and light trapping in a broad spectrum, leading to a 22% improvement in power conversion efficiency of the nc-Si:H thin-film solar cells compared to unstructured flat devices. By systematically analyzing the light-scattering properties of the back reflector containing the array of 3DM structures (called the 3DM back reflector hereafter) through optical experiments and theoretical studies using finite-difference time-domain (FDTD) simulations, we identified that the improved device performance mainly originates from the multiple plasmon resonances in our 3DM back reflector. In addition to the multiple plasmon resonances, we found that our 3D solar cell also exhibits an antireflection effect by the 3DM-structured top surface which boosts the light absorption in the nc-Si:H film, resulting in a highly enhanced external quantum efficiency (EQE) over a broad spectral range from 350–1100 nm where the nc-Si:H film is optically active.

2. Experimental details

2.1. Fabrication of 3DM structures

Using the multi-pin spark discharge generator (schematic illustration in online figure S1, stacks.iop.org/NANO/27/055403/mmedia), charged Ag nanoparticles and nitrogen ions were generated by spark discharge between Ag pin electrodes biased at 5 kV and a grounded Ag plate electrode with plural holes in the spark discharge chamber. Additional positive ions were produced by corona discharge between a tungsten pin electrode biased at 3.5 kV and a grounded tungsten plate electrode in the corona discharge chambers. The generated charged nanoparticles and ions were transported into the deposition chamber with the flow rate of the carrier gas (3 lpm per hole) and deposited on the Si substrate biased at −4 kV for 120 min. Under the experimental conditions, the 3DM structure arrays were fabricated using IAAL.

2.2. Optical simulations

Electromagnetic modeling was performed using Lumerical FDTD simulation software (www.lumerical.com). The simulation models are based on measured results of the actual device via scanning electron microscopy (SEM) and atomic force microscopy as shown in online figures S2 and S3. The refractive indices of the aluminum-doped zinc oxide (ZnO:Al), nc-Si:H, and indium tin oxide (ITO) films were taken from spectroscopic ellipsometry measurements, and the dielectric functions of Ag were adopted from Palik [31]. Since the 3DM structures were arrayed with a period of 2 μm, all optical simulations were performed for a single unit cell (over a 2 μm × 2 μm region) with periodic boundary conditions for the x- and y-axes, and with the perfectly matched layer (PML) condition for the z-axis in the 350–1100 nm spectral range.

2.3. Fabrication of solar cells

n–i–p substrate-type nc-Si:H solar cells were prepared onto the back reflectors using plasma-enhanced chemical vapor deposition (PECVD). The intrinsic and doped layers were deposited using a 60 MHz very high frequency and a 13.56 MHz radio frequency glow discharge, respectively. The 500 nm thick intrinsic nc-Si:H layers were deposited at a plasma density of 0.1 W cm^{-2}. The thicknesses of the p- and n-doped layers were 15 and 30 nm, respectively. The substrate temperature and chamber pressure were fixed at 150 °C and 300 mTorr, respectively. The silane concentration ratio SC = [SiH_4]/([SiH_4] + [H_2]) was maintained at 5.5%. For p- and n-doping, B_2H_6 (1% in H_2) and PH_3 (1% in H_2) gases were added to SiH_4, H_2, and CH_4 (50% in H_2), respectively. The individual solar cells, which had areas of 0.3 cm × 0.3 cm, were defined using a shadow mask during the ITO film deposition. The Al metal grids were deposited using thermal evaporation.

2.4. Characterization of solar cells

The performance of the solar cells was measured at 25 °C by current density–voltage (J–V) measurement under 1 Sun (AM 1.5, 100 mW cm^{-2}) solar simulator radiation. The open-circuit voltage (V_{oc}), short-circuit current density (J_{sc}), and fill factor (FF) were used to calculate the conversion efficiency of the solar cells. The EQE was obtained from spectral response measurements in the range of 350–1100 nm.

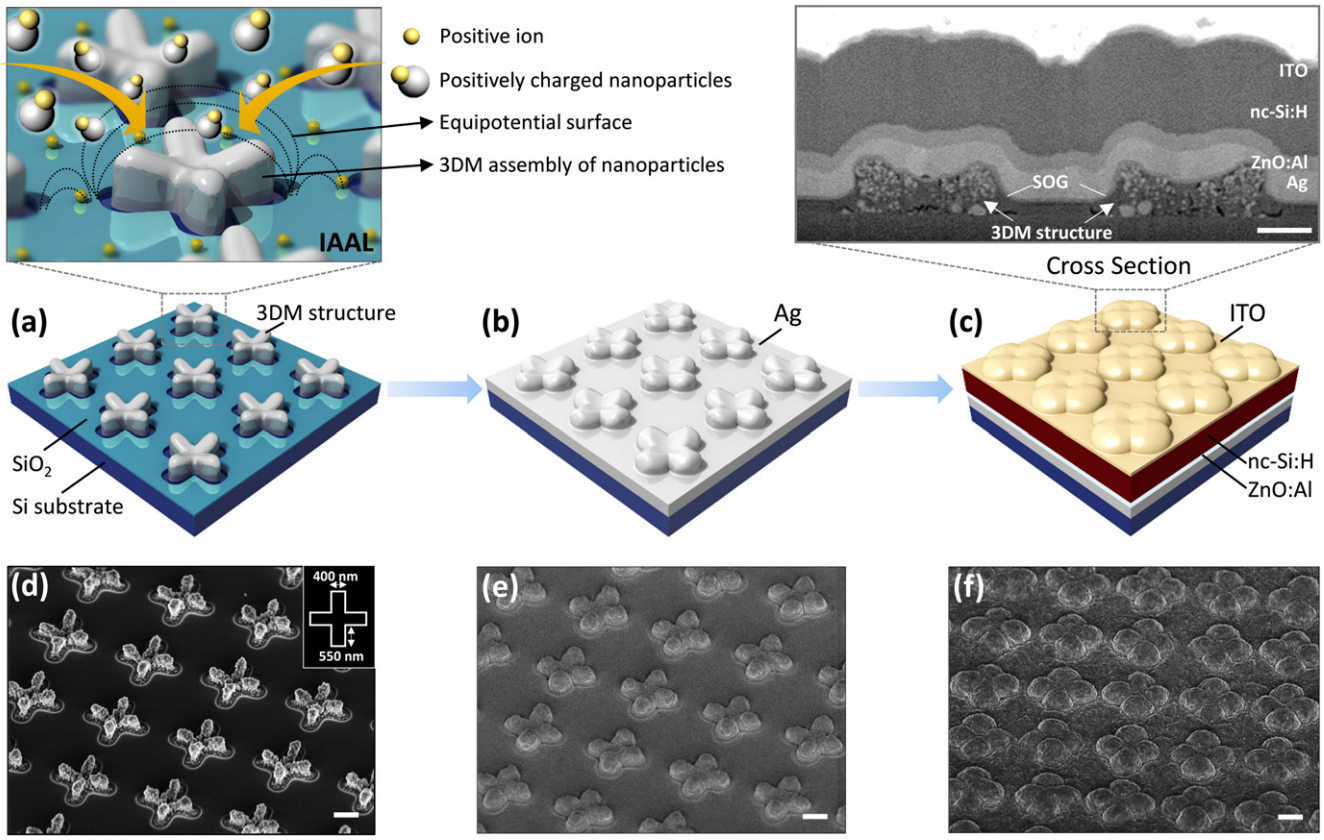

Figure 1. Schematized fabrication process of a nc-Si:H thin-film solar cell employing 3DM structure arrays. (a) The 3DM structures are fabricated by IAAL (the inset of figure 1(a)) with a multi-pin spark discharge method. The 3D solar cell is then produced on the 3DM structures by depositing (b) Ag, (c) ZnO:Al, nc-Si:H (n–i–p cell with a 500 nm thick intrinsic layer), and ITO layers. (d)–(f) SEM images showing each fabrication process of the 3D solar cell. The insets of figures 1(c) and (d) exhibit the cross section of the 3D solar cell and the physical dimension of the used SiO_2 pattern. All scale bars are 500 nm in length.

3. Results and discussion

The fabrication process of the 3D solar cell is illustrated in figure 1. IAAL with a multi-pin spark discharge method allows us to manufacture the sophisticated 3DM structures over a large area on the order of square centimeters. The multi-pin spark discharge generator produces positively charged Ag nanoparticles and nitrogen ions uniformly as depicted in figure S1. The generated nanoparticles and ions are injected into the deposition chamber and transported toward a Si substrate with a pre-patterned SiO_2 film along the flow of the nitrogen carrier gas. Due to their higher electrical mobility, the positive ions arrive earlier at the negatively biased Si substrate than the positively charged nanoparticles and are then accumulated on the insulating SiO_2 surface. These accumulated ions repel the following charged nanoparticles, inducing electrostatic lens effects to focus the charged nanoparticles to the disclosed regions of the Si substrate (see the inset of figure 1(a)). The deposited nanoparticles form 3DM structures as a result of an interplay between the repelling electric field from the accumulated ions on the SiO_2 surface and the enhanced field near the surface of the growing nanostructures. In our experiments, we first patterned a square array of cross-shaped cavities (figure 1(d) inset) in the 50 nm thick SiO_2 layer having a 2 μm period. Using this SiO_2 pattern, we then applied IAAL [20–29] with a multi-pin spark discharge method [27, 30] to fabricate the 3DM structure arrays as a template for the 3D solar cells, as shown in figure 1(d), followed by the electron-beam sintering process of the 3DM structures to coalesce aggregated nanoparticles for strengthening the 3DM structures [32]. Gaps between the 3DM structure and the SiO_2 pattern were filled by the spin-on-glass coating process to minimize defects that could occur in the nc-Si:H layer deposited on them [13, 33, 34]. Here, the 3DM structures with rounded edges (see the inset of figure 1(c)) play a crucial role in enhancing the light-trapping effect and reducing the loss in photocurrent generation of the 3D solar cell. A 200 nm thick Ag back electrode was then deposited on the 3DM structure arrays at an oblique angle via the thermal evaporation process to achieve the conformal Ag film along the surface morphology of the 3DM structures. Subsequently, a 130 nm thick ZnO:Al layer was sputtered and the n–i–p nc-Si:H stack with a 500 nm thick intrinsic layer was deposited using PECVD, followed by sputtering an 80 nm thick ITO front electrode. The surface texture of 3DM structures was replicated on the Ag back reflector and on the ITO front electrode without noticeable differences due to the conformal film deposition, which causes 3DM texturing of the back reflector (figures 1(b) and (e)) and the front electrode (figures 1(c) and

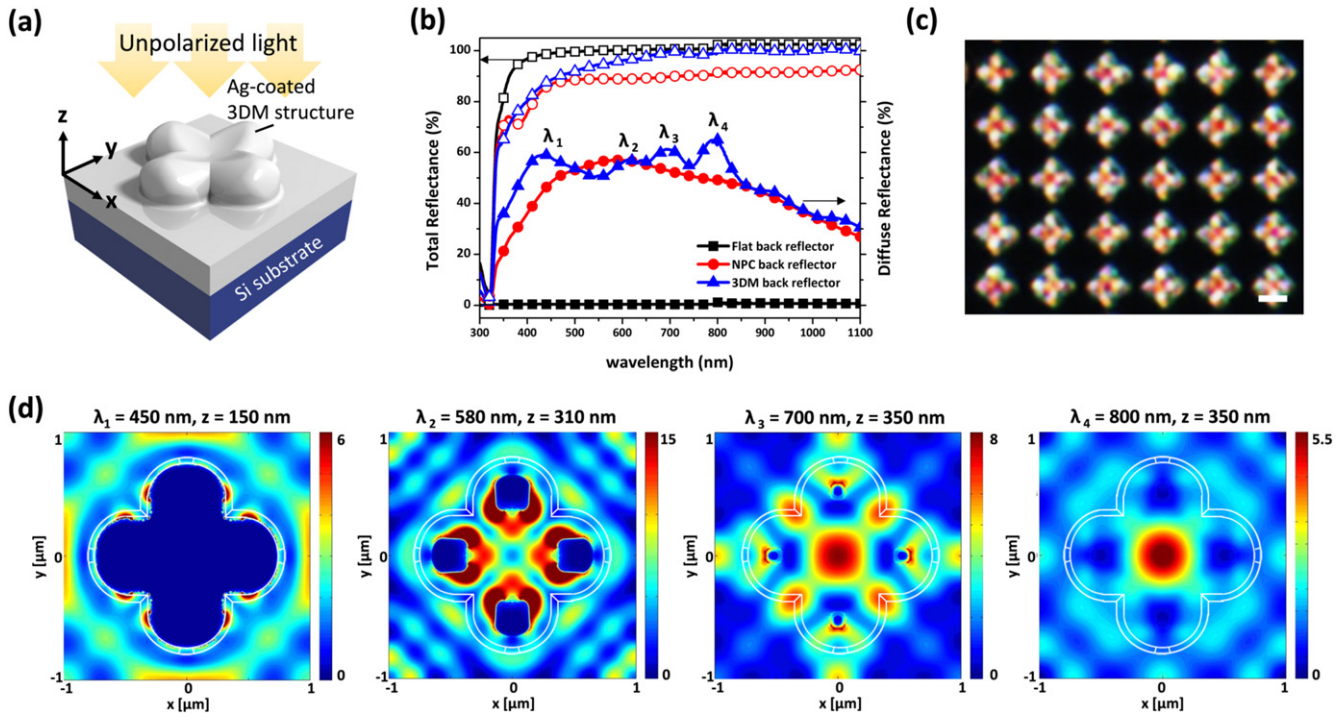

Figure 2. (a) An illustrated simulation model of the 3DM back reflector based on the Ag-coated 3DM structures. (b) Measured total and diffuse reflectance spectra of the flat (black squares), the NPC (red dots), and the 3DM (blue triangles) back reflectors. (c) A dark-field image (scale bar: 1 μm) and (d) electric field intensity profiles of the 3DM back reflector at the four wavelengths (λ_1–λ_4 in figure 2(b)).

(f)). In this study, we determined the suitable morphology and size of the 3DM back reflector for the nc-Si:H thin-film (~500 nm) solar cell by adjusting the deposition times of the 3DM structures as well as the deposition angles of the Ag back electrodes (see online figures S4 and table S1). All nc-Si:H thin-film solar cells with or without 3DM structures were produced under the same fabrication conditions.

The fabricated 3DM structures have a sophisticated geometric shape with varying dimensions from the nano- to micro-scale not only in the *x*- and *y*-directions, but also in the *z*-direction as illustrated in figure 2(a), which is difficult to realize employing other lithographic methods. To study how this multiscale feature of the 3DM structures improves light-scattering properties as a new type of 3DM back reflector, we measured the diffuse reflectance using a UV–vis–NIR spectrophotometer (Cary 5000, Agilent Technologies), and obtained a dark-field image (BX51 and DP73, Olympus) of the 3DM back reflector as presented in figures 2(b) and (c), respectively. The diffuse reflectance of the 3DM back reflector ranges from 50%–70% over the entire visible spectrum, showing that the 3DM structures scatter the incident light efficiently. More interestingly, this diffuse reflectance spectrum exhibits plural peaks at 450, 580, 700, and 800 nm, which are primarily attributed to the multiple plasmon resonances of the 3DM structures. The dark-field image displayed in figure 2(c) also shows multiple colors at different sites of the 3DM back reflector, revealing that the enhancement in scattering is induced by localized resonant processes [35]. In order to fully understand the multiple plasmon resonances of the 3DM structures, we performed full wave electromagnetic simulations using the FDTD method. Figure 2(d) shows the simulated profiles of electric field intensity in the *x*–*y*-plane at each resonance wavelength obtained from the diffuse reflectance spectrum. The calculated electric field is concentrated at the side walls of the petals, the top surfaces of the petals, and the center of the structure for blue-green (450 nm), yellow (580 nm), and red (700 and 800 nm) lights, respectively, which corresponds well to the experimental dark-field image shown in figure 2(c). The strong near-field enhancement near the metal surface is a clear indication of the surface plasmon resonance. The resonance wavelengths can easily be tuned by changing the morphologies and dimensions of the 3DM structures by controlling the shapes and sizes (including lengths, widths, periods, and thicknesses) of the insulating pre-patterns and deposition times [20–29]. The multiple plasmon resonances originating from the multiscale feature of the 3DM structures boost the light scattering and absorption efficiency in the multi-spectral range, together with increased diffuse reflectance due to the textured surface of the 3DM back reflector. Thus, this makes our 3DM back reflector appealing for solar cell applications.

To prove the superior light-trapping behavior of our 3DM back reflector, we compared the reflectance of the 3DM back reflector with that of the flat Ag film and the back reflector employing randomly distributed nanoparticle clusters (NPCs). The NPCs were prepared using the spin-coating process of silica nanoparticles with a diameter of 200 nm equivalent to the minimum dimension of the top-view 3DM structure. The surface coverage for both the NPCs and the 3DM structures was chosen to be approximately equal to 12%

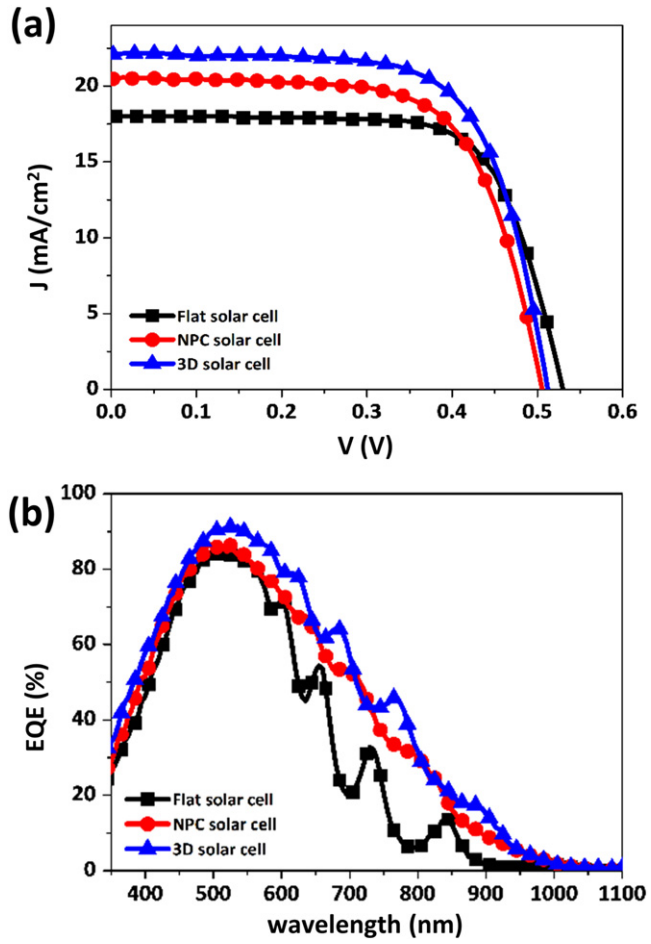

Figure 3. (a) *J*–*V* curves and (b) EQEs of the flat (black squares), the NPC (red dots), and the 3D (blue triangles) solar cells.

(see online figure S5). An Ag film was then deposited on the NPCs to fabricate the NPC back reflector through the same approach as used for the 3DM back reflector. Figure 2(b) shows the measured total and diffuse reflectance curves of the three back reflectors. The total reflectance of the flat Ag film is only given by the specular reflectance because diffuse reflectance is close to zero, while for the 3DM and the NPC back reflectors, much enhanced diffuse reflectance is observed. Here, it is noted that the 3DM back reflector reveals higher total (lower parasitic absorption loss) and diffuse (higher scattering property) reflectance than those of the NPC back reflector even with the same percentage of surface coverage. These results demonstrate that the 3DM back reflector traps light better than the NPC back reflector due to its multiple plasmon resonances. Furthermore, the useful features of IAAL, including precise controllability with nanoscale resolution over 3DM structure structuring, wavelength tunability, and reproducibility, make the 3DM back reflector superior to the other back reflectors.

To quantify the light-trapping effects of 3DM structures on device performance, we measured the *J*–*V* characteristics and the EQEs of the three different types of nc-Si:H thin-film (~500 nm) solar cells fabricated on the flat structure, the NPCs, and the 3DM structures as shown in figures 3(a) and (b). Table 1 summarizes the performance parameters of each device. J_{sc} of the devices increases from 17.1 mA cm^{-2} for the flat solar cell to 20.5 and 22.1 mA cm^{-2} for the NPC and the 3D solar cells, respectively. Such a difference in J_{sc} improvement is explained by higher EQE enhancement in the 3D solar cell in the wide wavelength range from 350 to 1100 nm relative to that of the NPC solar cell as shown in figure 3(b). Here, it is noted that the increase in the J_{sc} of the 3D solar cell mainly originates from the EQE enhancement in the red and near-infrared regions with a small but noticeable increase in the UV and visible ranges and, even with a much thinner nc-Si:H absorber layer, the J_{sc} value of the 3D solar cell is comparable with that (20–23 mA cm^{-2}) of nc-Si:H thin-film (1–1.5 μm) solar cells using randomly textured back reflectors, photonic crystals, and plasmonic structures in previous studies [36–42]. Moreover, since V_{oc} and the FF of the 3D solar cell are comparable to those of the flat cell, it is found that the 3DM structures do not undermine the electrical performance of the device even with an average 21.4% increase in surface area compared to the flat structures (see online figure S6 and table S2). Consequently, a 22% increase in efficiency of the 3D solar cell results from the significantly enhanced J_{sc}, which is higher than the case of the NPC solar cell which achieves only a 9% increase with respect to the flat cell.

To identify the origin of the superior light-trapping performance of the 3D solar cell, we analyzed how the surface textures of the 3DM front electrode and the 3DM back reflector individually enhance the optical characteristics of the solar cell using electromagnetic simulations. We first compared the optical transmittance of a flat and the 3DM front electrode employed in our device. In order to isolate the effect of the front electrode, here we investigated the transmittance through the front surface of the structure (see the inset of figure 4(a)) with an infinitely thick lossless active layer ($n = 3.8$ and $k = 0$). Figure 4(a) indicates that the 3DM textured front electrode exhibits superior transmittance over the flat one for the entire spectrum with a maximum enhancement of nearly 9%, except around 550 nm where the impact of the 3DM texturing on the transmittance is negligible due to the ITO layer satisfying an antireflection condition at the air–nc-Si:H interface [43]. This enhanced transmittance at wide wavelengths originates from the gradient refractive index profiles and the multiscale feature of the 3DM front electrode [44]. We then investigated the light-scattering properties of the 3DM back reflector covered by ZnO:Al and an infinitely thick lossless nc-Si:H layer (see the inset of figure 4(b)). Similar to the measured diffuse reflectance spectrum of the bare Ag 3DM back reflector (figure 2(b)), the calculated scattering spectrum presented in figure 4(b) shows multiple plasmon peaks at 460, 590, 740, and 950 nm, which are slightly red-shifted due to the higher index of the surrounding materials [45]. In order to see how these multiple plasmon resonances affect the light absorption in the actual device, we also simulated the full-device structure with experimental dielectric functions of the nc-Si:H layer measured by ellipsometry. Assuming that the absorbed photons in the active layer are fully converted to electron–

Table 1. Performance parameters of nc-Si:H thin-film (layer thickness = ~500 nm) solar cells fabricated in this study.

	J_{sc} (mA cm^{-2})	V_{oc} (V)	FF (%)	Efficiency (%)
Flat solar cell	17.1 ± 0.4	0.53 ± 0.01	70.9 ± 0.7	6.4 ± 0.2
NPC solar cell	20.5 ± 0.5	0.51 ± 0.01	67.5 ± 0.7	7.0 ± 0.2
3D solar cell	22.1 ± 0.6	0.51 ± 0.01	68.7 ± 0.7	7.8 ± 0.3

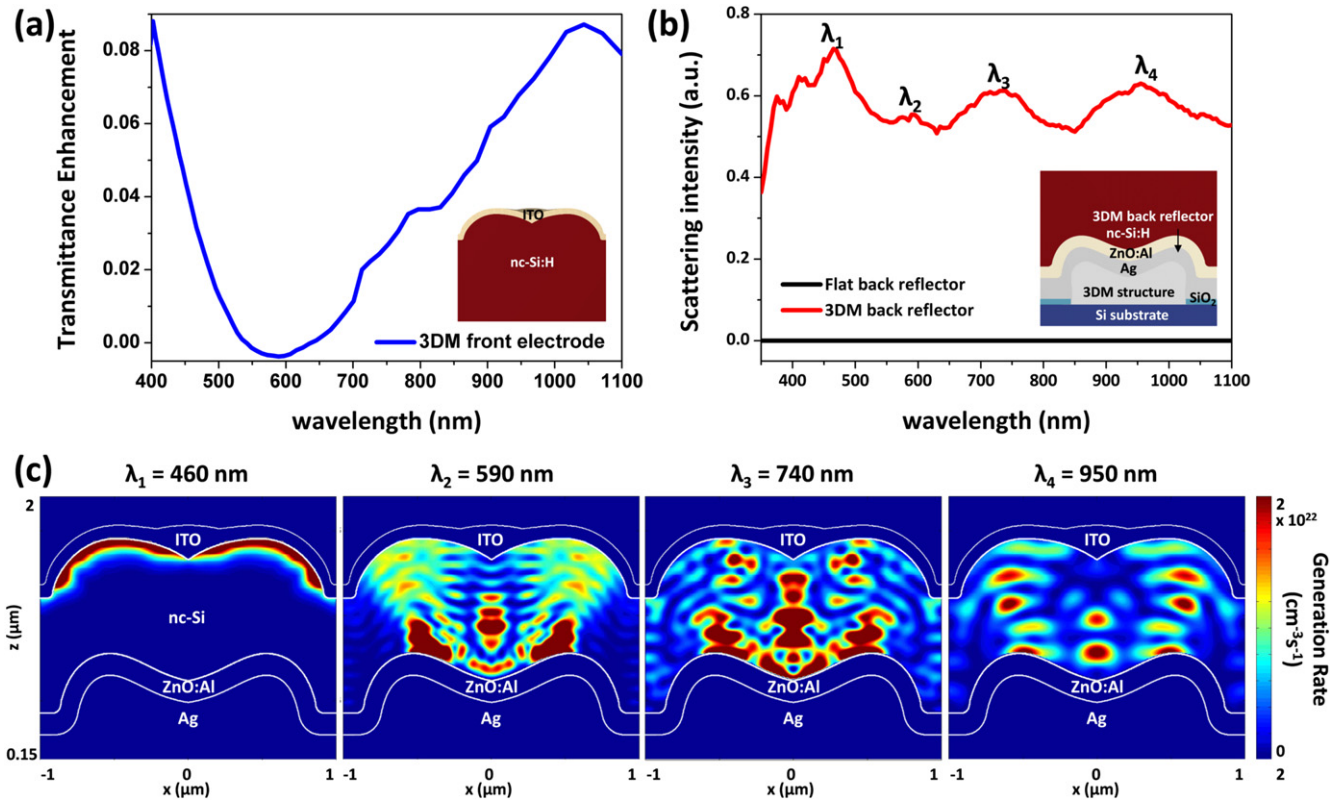

Figure 4. (a) Transmittance enhancement in nc-Si:H (blue line) induced only by the 3DM front electrode (inset). (b) Scattering intensities of the flat (black line) and the 3DM (red line, inset) back reflectors. (c) Cross-sectional spatial distributions of carrier generation rates in nc-Si:H of the 3D solar cell at the four wavelengths (λ_1–λ_4 in figure 4(b)).

hole pairs, we calculated the carrier generation rate by

$$G(\lambda) = \frac{\varepsilon'' |E|^2}{2\hbar}$$

where ε'' is the imaginary part of the permittivity and E is the electric field [11, 12]. Figure 4(c) illustrates the spatial profiles of $G(\lambda)$ at the plasmon resonance wavelengths of 460, 590, 740, and 950 nm. The localized mode of the generation rate is observed only at the front portion of nc-Si:H at 460 nm. On the other hand, the widely distributed profiles of high carrier generation rates in the nc-Si:H are observed at 590, 740, and 950 nm. The localized generation rate profiles near the back portion of the nc-Si:H indicate that the multiple plasmon resonances of the 3DM back reflector lead to strong near-field enhancement in the nc-Si:H. In addition to these multiple plasmon resonances, the 3DM-structure-induced light scattering and antireflection provide further enhancement in light-trapping efficiency. Thus, it is found that both the 3DM front electrode and the 3DM back reflector induce an increase in light absorption over the entire spectral range where the nc-Si:H is optically active. Here, the 3DM back reflector with multiple plasmon resonances mainly enhances the light-trapping efficiency in the red and the near-infrared regions of the spectrum. Only the antireflection effect from the 3DM front electrode improves the blue response of the 3D solar cell because the light is entirely absorbed within nc-Si:H before it reaches to the back reflector due to the highly absorbing feature of nc-Si:H in the blue spectral region [46]. All corresponding light absorption enhancements in the nc-Si:H boost the photocurrent and thereby high power conversion efficiency in the 3D solar cell.

4. Conclusions

We have fabricated sophisticated 3DM structure arrays over a large area under atmospheric conditions, whose multiscale features induce plasmon resonances at multiple frequencies, using IAAL in conjunction with a multi-pin spark discharge method. Using this 3DM plasmonic light-trapping

architecture, we have accomplished a 22% and an 11% increase in the efficiency of the nc-Si:H thin-film solar cell compared to the devices employing a flat structure and NPCs, respectively. The multiple plasmon resonances of our 3DM structures, in addition to the antireflection effect of the 3DM textured front electrode, provide significant enhancement in light absorption over the wide spectral range from 350–1100 nm, which leads to a 30% increase in photocurrent relative to the flat cell. Moreover, even with a much thinner intrinsic nc-Si:H layer, the J_{sc} of the 3D solar cell shows a comparable value to that of the nc-Si:H thin-film (1–1.5 μm) solar cells utilizing various types of textured back reflectors. Since the presented IAAL with a multi-pin spark discharge method provides a reliable and versatile route to large-area 3DM fabrication, it will add new degrees of freedom in designing future energy devices incorporating 3DM structures.

Acknowledgements

This work was supported by the Global Frontier R&D Program on Center for Multiscale Energy System (Grant no. 2011-0031561, 2011-0031567 and 2012M3A6A7054855) by the National Research Foundation (NRF) under the Ministry of Science, ICT and Future Planning, Korea. The authors thank Dr Sei Jin Park for insightful discussions.

References

[1] Shah A, Torres P, Tscharner R, Wyrsch N and Keppner H 1999 Photovoltaic technology: the case for thin-film solar cells *Science* **285** 692–8

[2] Ferry V E, Verschuuren M A, Li H B T, Verhagen E, Walters R J, Schropp R E I, Atwater H A and Polman A 2010 Light trapping in ultrathin plasmonic solar cells *Opt. Express* **18** A237–45

[3] Söderström K, Escarré J, Cubero O, Haug F J, Perregaux S and Ballif C 2011 UV-nano-imprint lithography technique for the replication of back reflectors for n–i–p thin film silicon solar cells *Prog. Photovolt. Res. Appl.* **19** 202–10

[4] Kim J, Battaglia C, Charrière M, Hong A, Jung W, Park H, Ballif C and Sadana D 2014 9.4% efficient amorphous silicon solar cell on high aspect-ratio glass microcones *Adv. Mater.* **26** 4082–6

[5] Tanaka Y, Ishizaki K, De Zoysa M, Umeda T, Kawamoto Y, Fujita S and Noda S 2015 Photonic crystal microcrystalline silicon solar cells *Prog. Photovolt. Res. Appl.* **23** 1475–83

[6] Atwater H A and Polman A 2010 Plasmonics for improved photovoltaic devices *Nat. Mater.* **9** 205–13

[7] Chen S-C *et al* 2014 Toward omnidirectional light absorption by plasmonic effect for high-efficiency flexible nonvacuum Cu(In,Ga)Se2 thin film solar cells *ACS Nano* **8** 9341–8

[8] Zheng D, Pang X, Wang M, He Y, Lin C and Lin Z 2015 Unconventional route to hairy plasmonic/semiconductor core/shell nanoparticles with precisely controlled dimensions and their use in solar energy conversion *Chem. Mater.* **27** 5271–8

[9] Kang M-G, Xu T, Park H J, Luo X and Guo L J 2010 Efficiency enhancement of organic solar cells using transparent plasmonic Ag nanowire electrodes *Adv. Mater.* **22** 4378–83

[10] Liu X, Wu B, Zhang Q, Yip J N, Yu G, Xiong Q, Mathews N and Sum T C 2014 Elucidating the localized plasmonic enhancement effects from a single Ag nanowire in organic solar cells *ACS Nano* **8** 10101–10

[11] Ferry V E, Polman A and Atwater H A 2011 Modeling light trapping in nanostructured solar cells *ACS Nano* **5** 10055–64

[12] Deceglie M G, Ferry V E, Alivisatos A P and Atwater H A 2012 Design of nanostructured solar cells using coupled optical and electrical modeling *Nano Lett.* **12** 2894–900

[13] Hsu C-M, Battaglia C, Pahud C, Ruan Z, Haug F-J, Fan S, Ballif C and Cui Y 2012 High-efficiency amorphous silicon solar cell on a periodic nanocone back reflector *Adv. Energy Mater.* **2** 628–33

[14] Mihi A, Beck F J, Lasanta T, Rath A K and Konstantatos G 2014 Imprinted electrodes for enhanced light trapping in solution processed solar cells *Adv. Mater.* **26** 443–8

[15] Baek S-W, Park G, Noh J, Cho C, Lee C-H, Seo M-K, Song H and Lee J-Y 2014 Au@Ag core–shell nanocubes for efficient plasmonic light scattering effect in low bandgap organic solar cells *ACS Nano* **8** 3302–12

[16] Lee D H, Kwon J Y, Maldonado S, Tuteja A and Boukai A 2014 Extreme light absorption by multiple plasmonic layers on upgraded metallurgical grade silicon solar cells *Nano Lett.* **14** 1961–7

[17] Lu L, Luo Z, Xu T and Yu L 2013 Cooperative plasmonic effect of Ag and Au nanoparticles on enhancing performance of polymer solar cells *Nano Lett.* **13** 59–64

[18] Yao K, Salvador M, Chueh C-C, Xin X-K, Xu Y-X, deQuilettes D W, Hu T, Chen Y, Ginger D S and Jen A K Y 2014 A general route to enhance polymer solar cell performance using plasmonic nanoprisms *Adv. Energy Mater.* **4** 1400206

[19] Li X, Choy W C H, Huo L, Xie F, Sha W E I, Ding B, Guo X, Li Y, Hou J, You J and Yang Y 2012 Dual plasmonic nanostructures for high performance inverted organic solar cells *Adv. Mater.* **24** 3046–52

[20] Kim H, Kim J, Yang H, Suh J, Kim T, Han B, Kim S, Kim D S, Pikhitsa P V and Choi M 2006 Parallel patterning of nanoparticles via electrodynamic focusing of charged aerosols *Nat. Nanotechnol.* **1** 117–21

[21] You S and Choi M 2007 Numerical simulation of microscopic motion and deposition of nanoparticles via electrodynamic focusing *J. Aerosol Sci.* **38** 1140–9

[22] Lee H, You S, Woo C G, Lim K, Jun K and Choi M 2009 Focused patterning of nanoparticles by controlling electric field induced particle motion *Appl. Phys. Lett.* **94** 053104

[23] You S, Han K, Kim H, Lee H, Woo C G, Jeong C, Nam W and Choi M 2010 High-resolution, parallel patterning of nanoparticles via an ion-induced focusing mask *Small* **6** 2146–52

[24] Kim D, Pikhitsa P V, Yang H and Choi M 2011 Room temperature CO and H_2 sensing with carbon nanoparticles *Nanotechnology* **22** 485501

[25] Lee H, You S, Pikhitsa P V, Kim J, Kwon S, Woo C G and Choi M 2011 Three-dimensional assembly of nanoparticles from charged aerosols *Nano Lett.* **11** 119–24

[26] Woo C G, Shin H, Jeong C, Jun K, Lee J, Lee J-R, Lee H, You S, Son Y and Choi M 2011 Selective nanopatterning of protein via ion-induced focusing and its application to metal-enhanced fluorescence *Small* **7** 1790–4

[27] Ha K, Choi H, Jung K, Han K, Lee J-K, Ahn K and Choi M 2014 Large-area assembly of three-dimensional nanoparticle structures via ion assisted aerosol lithography with a multi-pin spark discharge generator *Nanotechnology* **25** 225302

[28] Jung K, Hahn J, In S, Bae Y, Lee H, Pikhitsa P V, Ahn K, Ha K, Lee J-K, Park N and Choi M 2014 Hotspot-

engineered 3D multipetal flower assemblies for surface-enhanced raman spectroscopy *Adv. Mater.* **26** 5924–9
[29] Choi H, Kang S, Jung W, Jung Y-h, Park S J, Kim D S and Choi M 2015 Controlled electrostatic focusing of charged aerosol nanoparticles via an electrified mask *J. Aerosol Sci.* **88** 90–7
[30] Han K, Kim W, Yu J, Lee J, Lee H, Gyu Woo C and Choi M 2012 A study of pin-to-plate type spark discharge generator for producing unagglomerated nanoaerosols *J. Aerosol Sci.* **52** 80–8
[31] Palik E D 1998 *Handbook of Optical Constants of Solids* vol 3 (New York: Academic)
[32] Ha K 2015 Large-area assembly and restructuring of multiscale multidimensional nanoparticle structures and their application to a solar cell *PhD dissertation*, Seoul National University
[33] Li H B T, Franken R H, Rath J K and Schropp R E I 2009 Structural defects caused by a rough substrate and their influence on the performance of hydrogenated nano-crystalline silicon n–i–p solar cells *Sol. Energy Mater. Sol. Cells* **93** 338–49
[34] Python M, Madani O, Dominé D, Meillaud F, Vallat-Sauvain E and Ballif C 2009 Influence of the substrate geometrical parameters on microcrystalline silicon growth for thin-film solar cells *Sol. Energy Mater. Sol. Cells* **93** 1714–20
[35] Maier S A and Atwater H A 2005 Plasmonics: localization and guiding of electromagnetic energy in metal/dielectric structures *J. Appl. Phys.* **98** 011101
[36] Sai H, Fujiwara H and Kondo M 2009 Back surface reflectors with periodic textures fabricated by self-ordering process for light trapping in thin-film microcrystalline silicon solar cells *Sol. Energy Mater. Sol. Cells* **93** 1087–90
[37] Smirnov V, Böttler W, Lambertz A, Wang H, Carius R and Finger F 2010 Microcrystalline silicon n–i–p solar cells prepared with microcrystalline silicon oxide (μc-SiOx:H) n-layer *Phys. Status Solidi* C **7** 1053–6
[38] Biswas R, Bhattacharya J, Lewis B, Chakravarty N and Dalal V 2010 Enhanced nanocrystalline silicon solar cell with a photonic crystal back-reflector *Sol. Energy Mater. Sol. Cells* **94** 2337–42
[39] Paetzold U W, Moulin E, Michaelis D, Böttler W, Wächter C, Hagemann V, Meier M, Carius R and Rau U 2011 Plasmonic reflection grating back contacts for microcrystalline silicon solar cells *Appl. Phys. Lett.* **99** 181105
[40] Sai H and Kondo M 2011 Light trapping effect of patterned back surface reflectors in substrate-type single and tandem junction thin-film silicon solar cells *Sol. Energy Mater. Sol. Cells* **95** 131–3
[41] Marins E, Warzecha M, Michard S, Hotovy J, Böttler W, Alpuim P and Finger F 2014 Flexible n–i–p thin film silicon solar cells on polyimide foils with textured ZnO:Ga back reflector *Thin Solid Films* **571** Part 1 9–12
[42] Meier M, Paetzold U W, Prömpers M, Merdzhanova T, Carius R and Gordijn A 2014 UV nanoimprint for the replication of etched ZnO:Al textures applied in thin-film silicon solar cells *Prog. Photovolt. Res. Appl.* **22** 1226–36
[43] Sai H, Jia H and Kondo M 2010 Impact of front and rear texture of thin-film microcrystalline silicon solar cells on their light trapping properties *J. Appl. Phys.* **108** 044505
[44] Raut H K, Ganesh V A, Nair A S and Ramakrishna S 2011 Anti-reflective coatings: a critical, in-depth review Energy *Environ. Sci.* **4** 3779–804
[45] Jensen T R, Duval M L, Kelly K L, Lazarides A A, Schatz G C and Van Duyne R P 1999 Nanosphere lithography: effect of the external dielectric medium on the surface plasmon resonance spectrum of a periodic array of silver nanoparticles *J. Phys. Chem.* B **103** 9846–53
[46] Shah A V, Schade H, Vanecek M, Meier J, Vallat-Sauvain E, Wyrsch N, Kroll U, Droz C and Bailat J 2004 Thin-film silicon solar cell technology *Prog. Photovolt. Res. Appl.* **12** 113–42